Fatty acid metabolism complements glycolysis in the selective regulatory T cell expansion during tumor growth

Ilenia Pacella, Claudio Procaccini, Chiara Focaccetti, Stefano Miacci, Eleonora Timperi, Deriggio Faicchia, Martina Severa, Fabiana Rizzo, Eliana Marina Coccia, Fabrizia Bonacina, et al.

Fatty acid metabolism complements glycolysis in the selective regulatory T cell expansion during tumor growth

Ilenia Pacella[1], Claudio Procaccini[2], Chiara Focaccetti[1], Stefano Miacci[1], Eleonora Timperi[1], Deriggio Faicchia[2], Martina Severa[3], Fabiana Rizzo[3], Eliana Coccia[3], Fabrizia Bonacina[4], Nico Mitro[5], Giuseppe Norata[4], Grazisa Rossetti[6], V. Ranzani[6], M. Pagani[7], Ezio Giorda[8], Yu Wei[9], Giuseppe Matarese[10], Vincenzo Barnaba[11], Silvia Piconese[1]

[1]Sapienza University of Rome, [2]IEOS-CNR, [3]Istituto Superiore di Sanità, [4]University of Milan, [5]DiSFeB, Dipartimento di Scienze Farmacologiche e Biomolecolari, Università degli Studi di Milano, Milano, 20133, Italy., [6]Istituto Nazionale Genetica Molecolare INGM, [7]Istituto Nazionale Genetica Molecolare (INGM) Romeo ed Enrica Invernizzi, [8]Bambino Gesù Children's Hospital - IRCCS, [9]institut Pasteur, [10]Università di Napoli Federico II, [11]university of rome

Submitted to Proceedings of the National Academy of Sciences of the United States of America

The tumor microenvironment restrains conventional T cell (Tconv) activation while facilitating the expansion of regulatory T cells (Tregs). Here we showed that Tregs advantage in the tumor milieu relies on supplemental energetic routes involving lipid metabolism. In murine models, tumor-infiltrating Tregs displayed intracellular lipid accumulation, which was attributable to an increased rate of fatty acid (FA) synthesis. Since relative advantage in glucose-uptake may fuel FA synthesis in intratumoral Tregs, we demonstrated that both glycolytic and oxidative metabolism concurred to Tregs expansion. We corroborated our data in human tumors showing that Tregs displayed a gene signature towards glycolysis and lipid synthesis. Our data support a model in which signals from the tumor microenvironment induce a circuitry of glycolysis, FA synthesis and oxidation that confers to Tregs a preferential proliferative advantage, whose targeting might represent a strategy for cancer treatment.

Treg | tumor microenvironment | glycolysis | fatty acid synthesis | ox40

Introduction

Regulatory T cells (Tregs), i.e., Foxp3-expressing CD4 T lymphocytes, are widely recognized as crucial controllers of immune responses, and the balance between Tregs and effector T cells determines the success of immune surveillance over cancer progression. Therefore, understanding the dynamics that dictate the relative Treg advantage over Tconvs is of utmost importance in the design of cancer immunotherapies (1). Both thymus-derived (tTregs) and peripherally induced (pTregs) subsets populate the tumor microenvironment (TME) (2): while the differentiation of pTregs (as well as of iTregs, in vitro induced) is favored in conditions of poor T cell proliferation, both pTregs and tTregs can actively proliferate in response to adequate signals (3, 4) and independently concur to generate the Treg pool in tumor-bearing hosts (5).

The T cell switch between quiescence and activation relies on a metabolic shift from oxidative to glycolytic pathways, respectively ensuring long-term survival and fuelling fast energy supply, biosynthesis and replication (6). Distinct cellular subsets display different metabolic signatures. Many pieces of evidence suggest that conventional T cells (Tconvs) require amplifying oxidative pathways, while blunting glycolysis, to undergo the terminal/restrained activation that ultimately favors their differentiation into iTreg/pTreg (7-9). First, mouse iTregs have been shown to preferentially use fatty acid oxidation (FAO) (7, 8, 10); however glycolysis is rather essential for human iTreg development upon suboptimal stimulation, since the "moonlighting" enzyme enolase-1 suppresses the transcription of the exon 2-containing FOXP3 splicing variant (FOXP3-E2, crucial determinant of the regulatory function), unless engaged in glycolysis (11).

The proliferation of pre-established Tregs may have completely distinct metabolic requirements, with respect to the conversion of Tconvs into iTregs/pTregs. Ex vivo, highly proliferative human Tregs show active mTOR and high levels of the glucose transporter Glut1; both glycolytic and FA-oxidative pathways concur to their expansion in vitro (12-14), and mTOR drives a lipogenic and cholesterogenic signature in Tregs, which crucially sustains their expansion in vivo (15). Overall, these data indicate that Tregs may arrange both glycolytic and oxidative routes and, similar to memory CD8 T cells (16), may also perform fatty acid synthesis (FAS). This may become especially true in contexts of limited nutrient availability such as the TME, where tumor cells subtract glucose to effector T cells thus blocking their glycolytic shift and anti-tumor activity (17, 18).

Here, we hypothesized that Tregs may overwhelm Tconvs in the hostile tumor context thanks to their peculiar ability to exploit supplemental metabolic routes and thus to optimize nutrient usage. We first documented that, in a mouse tumor model, tumor-infiltrating Tregs preferentially capture and utilize glucose not only to fuel glycolysis but also to synthesize and accumulate FAs, and Tregs relied on FAS and FAO to a higher extent than Tconvs in vitro. Genes involved in glycolysis and lipid biosynthesis are enriched in the signature of activated Tregs sorted from human liver cancer. Thus, exploiting a combination of different

Significance

Recent studies have established that metabolic restrains, such as glucose restriction, impair the activities of effector T cells in the tumor microenvironment. In the same context, a huge expansion of activated regulatory T cells in tumor tissues has been described in mice and humans, contributing to the suppression of protective anti-tumor immunity. Our data demonstrate that Tregs are committed to survive and proliferate in such a hostile milieu thanks to a metabolic advantage based on the combination of glycolysis and fatty acid synthesis and oxidation. This allows Treg to prevail over Tconv that rely primarily on the glycolytic pathway for their metabolic demands. The awareness of the metabolic dynamics of Treg in tumor could provide new means for cancer immunotherapy.

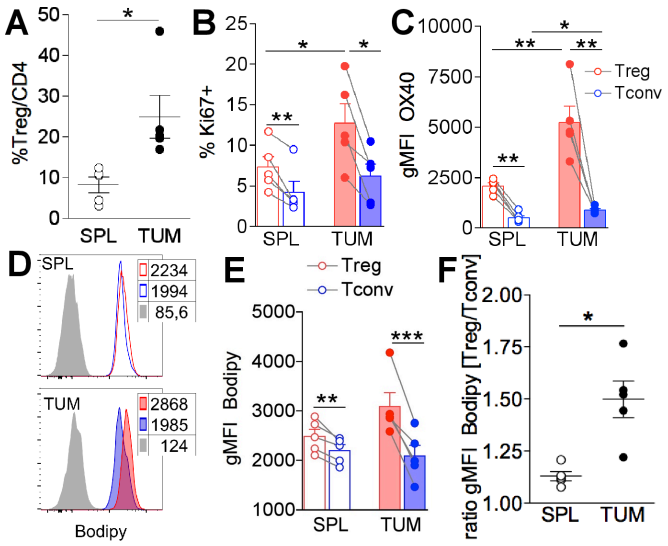

Fig. 1. *Expanded and activated tumor-infiltrating Tregs display high intracellular lipid content.* 5x10^5 MCA38 cells were injected s.c. into C57BL/6 mice, and flow cytometry analysis was performed on lymphocytes extracted from spleen (SPL) and tumor (TUM) after 14 days. **(A)** Frequency of CD25+Foxp3+ Tregs in gated CD4+ lymphocytes. **(B)** Frequency of cells expressing Ki67 and **(C)** geometric mean fluorescent intensity (gMFI) of OX40 in gated CD25+Foxp3+ Tregs (red) and CD25-Foxp3- Tconvs (blue) in SPL (empty bars) and TUM (filled bars) from tumor-bearing mice. **(D)** Representative histograms and **(E)** gMFI analysis of Bodipy incorporation in gated CD25+Foxp3+ Tregs (red) and CD25-Foxp3- Tconvs (blue) in SPL (empty peaks and bars) and TUM (solid peaks and bars) from tumor-bearing mice. Peaks in grey represent the fluorescence-minus-one (FMO) controls. **(F)** Ratio between Bodipy gMFI in Tregs and Tconvs from SPL and TUM.Error bars show mean ± SEM, each dot corresponds to a single mouse. Data shown are from a representative out of two independent experiments. *p < 0.05, **p < 0.01, ***p < 0.005, by Student t test, paired between Tregs and Tconvs in the same samples; unpaired, between populations of different samples.

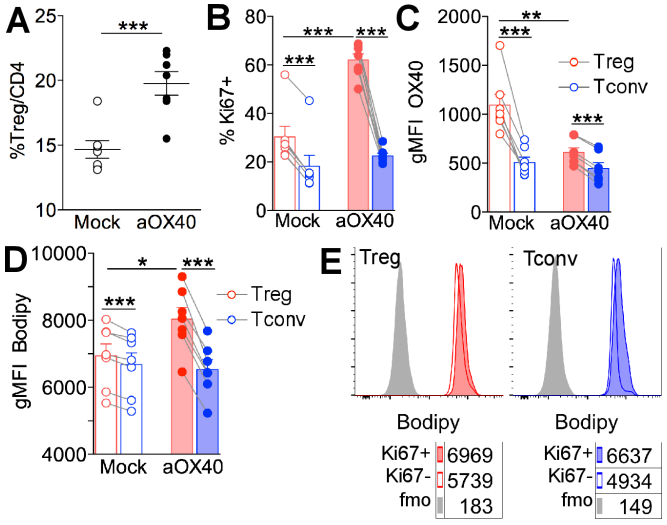

Fig. 2. *OX40 triggering alone recapitulates Treg proliferation and FA accumulation in vivo.* C57BL/6 naïve mice were injected i.p. with 500 µg of anti-OX40 agonist mAb (OX86) or PBS as mock control. After 6 days, flow cytometry analysis was performed in splenocytes. **(A)** Frequency of CD25+Foxp3+ Tregs in gated CD4+ lymphocytes. **(B)** Frequency of cells expressing Ki67, **(C)** geometric mean fluorescent intensity (gMFI) of OX40, and **(D)** gMFI analysis of Bodipy incorporation, in gated CD25+Foxp3+ Tregs (red) and CD25-Foxp3- Tconvs (blue) in aOX40-treated compared to mock-treated mice. **(E)** Representative histograms showing Bodipy labeling in gated Ki67+ or Ki67- Tregs or Tconvs; numbers indicate Bodipy gMFI; peaks in grey represent the fluorescence-minus-one (FMO) controls. Error bars show mean ± SEM, each dot corresponds to a single mouse; 6-7 mice were included in each experimental group. *p < 0.05, **p < 0.01, ***p < 0.005, by Student t test, paired between Tregs and Tconvs in the same samples; unpaired, between populations of different samples.

metabolic routes may be a novel immune escape mechanism that conveys to Tregs a selective advantage in the TME.

Results

Proliferating Tregs in the TME accumulate intracellular lipids.

In the visceral adipose tissue (VAT), expanded Tregs accumulate intracellular lipids under the cell-intrinsic control of the adipogenic factor PPARγ□(19). Therefore, we first checked whether lipid accumulation also occurred in another context of Treg expansion, i.e., the TME. To this aim, CD4+Foxp3+ Tregs were analyzed by flow cytometry, in comparison with CD4+Foxp3- Tconvs, in cells extracted from tumor beds (TUM), or from spleens as control (SPL), of C57BL/6 wild-type mice, bearing nodules of the subcutaneously implanted colon carcinoma cell line MCA38 (the gating strategy is shown in SI Appendix, **Fig. S1**). Confirming previous studies in a variety of mouse tumor models and in human cancers (1), Treg frequency was significantly increased at the tumor site **(Fig. 1A)**; compared to spleen cells and to Tconvs, TUM-Tregs were more proliferative, as pointed out by Ki67+ frequency **(Fig. 1B)**, and expressed higher levels of the receptor OX40 **(Fig. 1C)**, which we previously demonstrated to sustain Treg fitness in mouse models of homeostatic proliferation and colitis (20), and to promote the expansion of stable and suppressive Tregs in human cancers (21, 22).

When we stained the cells with Bodipy, a cell membrane-permeable fluorophore specific for neutral lipid stores, we could detect a higher intracellular lipid content in Tregs compared to Tconvs in both SPL and TUM **(Fig. 1D-E** and SI Appendix, **Fig. S1B)**; however, this phenomenon affected especially TUM-Tregs, as evidenced by a significantly increased ratio of Bodipy levels, between Tregs and Tconvs, in TUM compared to SPL **(Fig. 1F)**. Similar results were obtained in a distinct tumor model, i.e., the subcutaneously injected melanoma B16F10 (SI Appendix, **Fig. S2)**.

To ascertain whether the preferential lipid accumulation in Tregs was an exclusive feature of tumor, or was shared with other conditions characterized by Treg expansion, we analyzed Treg frequency and intracellular lipid content in two distinct models of liver disease, namely the *Mdr2*$^{-/-}$ mouse (developing from an early age inflammatory cholangitis that progresses into cirrhosis and cancer (23)), and the HCV-transgenic (HCVTg) mouse (spontaneously developing steatosis at advanced ages with no evidence of inflammation (24)). In young (3 weeks old) *Mdr2*$^{-/-}$ compared to wild-type mice, hepatic Tregs displayed a higher frequency, and this was again associated with greater intracellular lipid content in relation to Tconvs (SI Appendix, **Fig. S3A-C**); conversely, hepatic Tregs were not expanded in aged (>10 months old) HCVTg compared to wild-type mice, and no preferential lipid accumulation was detected in Tregs (SI Appendix, **Fig. S3D-F**). Overall these data indicate that Tregs enlarge their intracellular lipid pool when prompted to expansion, irrespective of whether triggered by inflammation- or tumor-associated stimuli.

We have previously demonstrated that OX40 plays non-redundant roles in Treg expansion in a variety of contexts including cancer (20, 21): therefore, we sought to test whether OX40 signal could induce lipid accumulation in proliferating Tregs. To this aim, we injected an anti-OX40 agonist mAb, OX86, in naïve mice: according to published data (25), OX40 triggering induced a huge increase of Treg frequency **(Fig. 2A)**. This expansion was likely due to the direct promotion of the selective proliferation of Tregs to the expense of Tconvs, as demonstrated by the increased percentage of Ki67+ Tregs, but not Ki67+ Tconvs **(Fig. 2B)**,

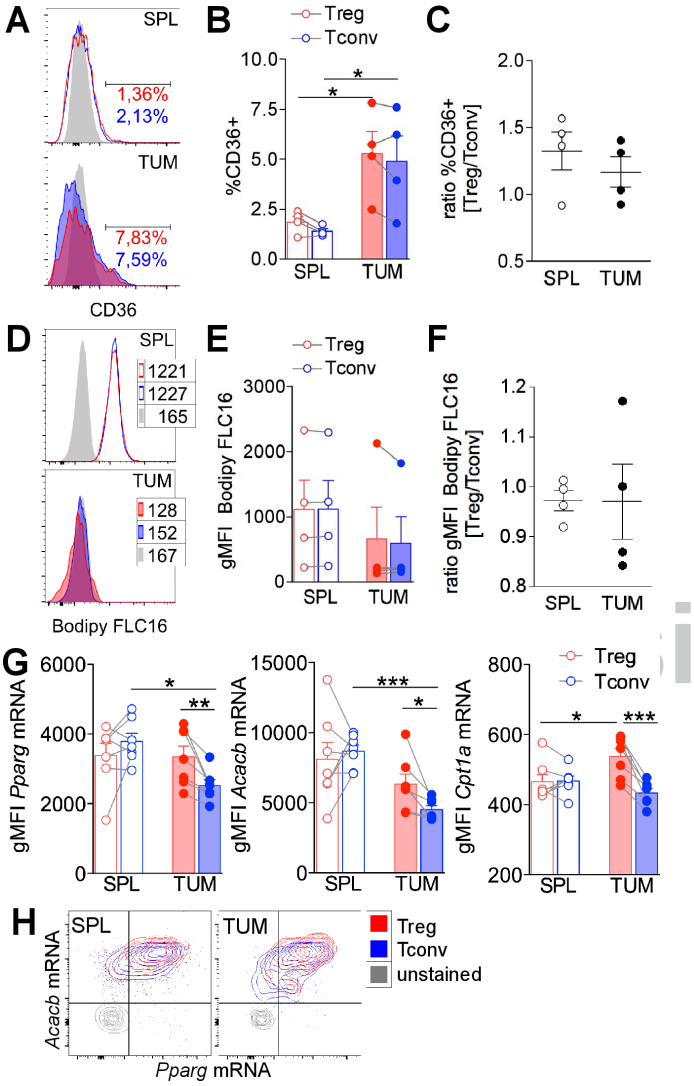

Fig. 3. *Fatty acid synthesis, rather than uptake, shapes the lipid Treg pool and contributes to Treg proliferation.* **(A-F)** Mice bearing tumors of 8x8 mm in size received an i.p. injection of the green fluorescent palmitate (Bodipy FL C16), 1 hour before spleen (SPL) and tumor (TUM) collection. Then Bodipy FL C16 uptake and CD36 expression were quantified by flow cytometry in CD25+Foxp3+ Tregs and CD25-Foxp3- Tconvs. **(A)** Representative histograms and **(B)** frequency of cells expressing CD36 in gated Tregs (red) and Tconvs (blue) in SPL (empty peaks and bars) and TUM (solid peaks and bars). **(C)** Ratio between frequency of CD36-expressing Tregs and Tconvs in SPL and TUM. **(D)** Representative histograms and **(E)** geometric mean fluorescence intensity (gMFI) of Bodipy FL C16 acquisition in gated Tregs (red) and Tconvs (blue) in SPL (empty peaks and bars) and TUM (solid peaks and bars). **(F)** Ratio between Bodipy FL C16 gMFI of Tregs and Tconvs in SPL and TUM tissue. Peaks in grey represent the fluorescence-minus-one (FMO) controls. **(G-H)** The expression level of *Pparg*, *Acacb* and *Cpt1a* mRNA was assessed in gated CD4+CD25+ Tregs and CD4+CD25- Tconvs was performed by PrimeFlow RNA assay. **(G)** Geometric mean fluorescence intensity of each gene expression in Tregs (red) and Tconvs (blue) in SPL (empty bars) and TUM (filled bars). **(H)** Representative overlay contour plots of *Acacb* and *Pparg* co-expressing cells in the indicated samples. Each dot corresponds to a single mouse; data shown are from a representative out of four independent experiments each including 3-7 mice per group. Error bars show mean ± SEM, *p < 0 .05, **p < 0 .01, by Student t test, paired between Tregs and Tconvs in the same sample; unpaired, between populations of different samples.

and also corroborated by the decreased OX40 staining ex vivo (with the same OX86 clone) of Tregs but not Tconvs of aOX40-treated mice (**Fig. 2C**). Notably, aOX40-induced Treg expansion

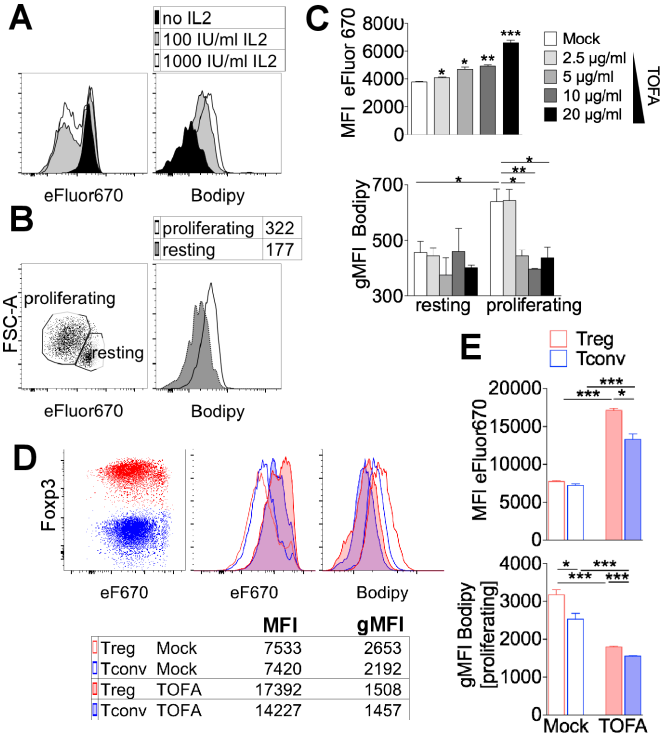

Fig. 4. *Inhibition of fatty acid synthesis blocks proliferation and lipid accumulation preferentially in Tregs in vitro.* **(A-C)** CD4+CD25+ Tregs, magnetically purified from splenocytes of naïve C57BL/6 mice, were labeled with eFluor670 and polyclonally stimulated for 4 days, then stained with Bodipy and analyzed by flow cytometry. **(A)** Representative histograms of eFluor670 dilution (left) and Bodipy incorporation (right) in Tregs cultured with different IL-2 concentrations. **(B)** Representative plot of proliferating and resting Treg gating strategy (left) and representative histogram of Bodipy incorporation within each gate (right). **(C)** Mean fluorescence intensity (MFI) of eFluor670 in gated Tregs (left), and geometric mean fluorescence intensity (gMFI) of Bodipy incorporation in gated resting and proliferating Tregs (right), cultured with different TOFA concentrations. **(D-E)** Magnetically purified Tregs and Tconvs were co-cultured at 1:1 ratio with feeder cells, anti-CD3 and IL-2, with or without TOFA (5 µg/ml). After 4 days, cells were stained with Bodipy and Foxp3, and flow cytometry analysis was performed in gated Tregs (Foxp3+, red) or Foxp3- (Tconvs, blue). **(D)** Representative overlay of Tregs and Tconvs in the indicated conditions; numbers indicate MFI of eFluor670 or gMFI of Bodipy. **(E)** Analysis of eFluor670 MFI or Bodipy gMFI (gated on proliferating cells) Tregs (red bars) or Tconvs (blue bars), either mock-treated (empty) or TOFA-treated (filled). Each condition was tested in triplicates; data shown are from a representative out of two independent experiments. Error bars show mean ± SEM, *p < 0.05, **p < 0.01, ***p < 0.005, by Student t test, unpaired.

was associated to a greater Bodipy staining of Tregs, which was even more pronounced in Ki67+ Tregs (**Fig. 2D-E**). These results strengthen the link between Treg proliferation and FA accumulation, and demonstrate that the sole OX40 engagement can trigger the selective proliferation of lipid-laden Tregs.

FA synthesis, rather than uptake, shapes the TUM-Treg lipid pool and promotes Treg proliferation.

In the adipose tissue, lipid-laden Tregs also display higher levels of the FA translocator CD36 (19); therefore, we tested whether a differential uptake of exogenous FAs might account for the higher lipid content in TUM-Tregs. We found that CD36 was modestly upregulated at the tumor site in both Tregs and Tconvs, but without any specific enrichment in TUM-Tregs (**Fig. 3A-C**). Then, we measured the absorption in vivo of a fluorescently labeled FA (Bodipy FL C16, a palmitic acid molecule conjugated to the Bodipy fluorophore), previously injected into tumor-bearing mice: both Tregs and Tconvs tended to acquire less

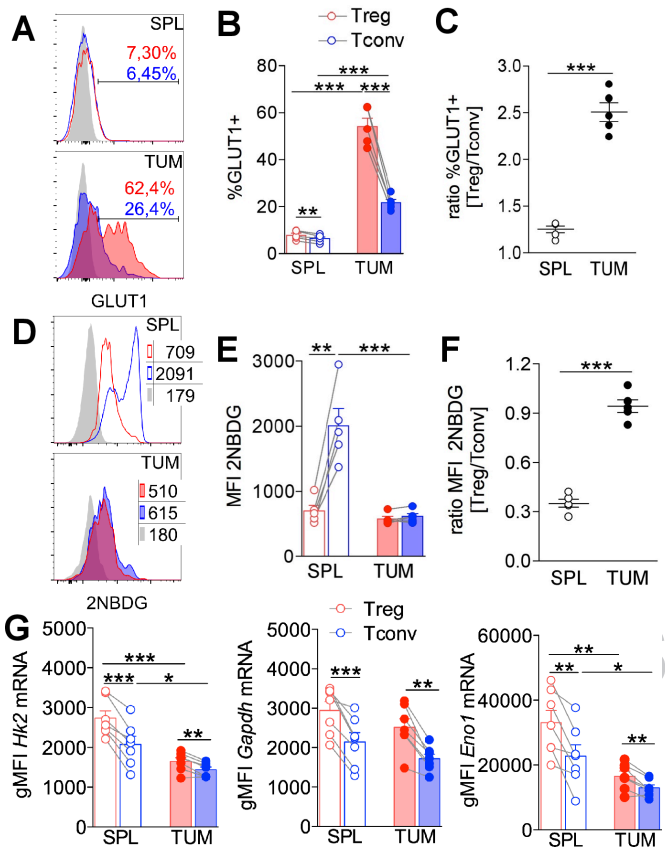

Fig. 5. *Glucose uptake and usage occurs preferentially in Tregs in tumors.* **(A-F)** Mice bearing tumors of 8x8 mm in size received an i.p. injection of the fluorescent glucose analogue 2-NBDG, and spleen (SPL) and tumor (TUM) were collected 15 minutes after injection. 2-NBDG uptake and GLUT1 expression were quantified by flow cytometry in CD25+Foxp3+ Tregs and CD25-Foxp3- Tconvs. **(A)** Representative histograms and **(B)** frequency of cells expressing GLUT1 in gated Tregs (red) and Tconvs (blue) in SPL (empty peaks and bars) and TUM (solid peaks and bars); grey peaks represent the fluorescence-minus-one (FMO) controls. **(C)** Ratio between frequency of GLUT1 expressing Tregs and Tconvs in SPL and TUM. **(D)** Representative histograms and **(E)** mean fluorescence intensity (MFI) of 2-NBDG acquisition in gated Tregs (red) and Tconvs (blue) in SPL (empty peaks and bars) and TUM (solid peaks and bars). **(F)** Ratio between 2-NBDG MFI of Tregs versus Tconvs at different sites. **(G)** Expression levels of the glycolysis-related genes *Hk2*, *Gapdh* and *Eno1*, evaluated through PrimeFlow RNA assay in gated CD4+CD25+ Tregs (red) and CD4+CD25- Tconvs (blue) from SPL (empty bars) and TUM (filled bars). Each dot corresponds to a single mouse; data shown are from a representative out of three independent experiments each including 3-7 mice. Error bars show mean ± SEM, *p < 0.05, **p < 0.01, ***p < 0.005, by Student t test, paired between Tregs and Tconvs in the same sample; unpaired, between populations of different samples.

FA in the tumor site compared to the spleen (despite the modest CD36 upregulation) but without any major difference between the two subsets (**Fig. 3D-F**). These results suggested a local defect in FA distribution and uptake, shared by Tregs and Tconvs and unrelated to their CD36 levels, and excluded preferential FA scavenging by TUM-Tregs: thus, we investigated whether intracellular FA metabolic routes were instead involved in lipid accumulation and proliferation of Tregs. First, we evaluated, in Tregs and Tconvs from tumor-bearing mice, the expression levels of 3 selected genes, *Pparg*, *Acacb* and *Cpt1a*, respectively required for FA storage, synthesis and oxidation. To this aim, we adopted PrimeFlow RNA Assay, allowing the simultaneous detection of transcripts and proteins by flow cytometry at single cell resolution. Thanks to this approach, we could detect that TUM-Tregs expressed all 3 genes at significantly higher levels

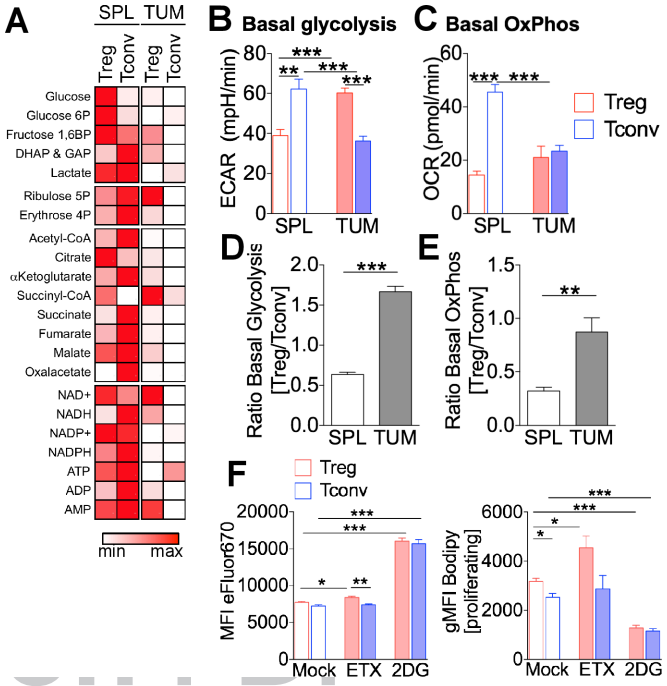

Fig. 6. *TUM-Treg display higher levels of both glycolytic and oxidative metabolism.***(A)** CD4+CD25+ Tregs and CD4+CD25- Tconvs were magnetically purified from pooled spleens and tumors of tumor-bearing mice, and metabolomic profiling was performed directly ex vivo by LC-MS/MS. The heatmap displays the levels of each metabolite (fg/cell) in the indicated samples (min/max related to each metabolite). **(B-E)** CD4+CD25+ Tregs and CD4+CD25- Tconvs were magnetically purified from pooled spleens and tumors of tumor-bearing mice, and quantification of extracellular acidification rate (ECAR) and oxygen consumption rate (OCR) were performed by Seahorse analysis after a 12-hours stimulation with anti-CD3/anti-CD28. **(B)** Basal glycolysis, **(C)** basal OxPhos, and **(D-E)** respective Treg/Tconv ratios for each index, in the indicated conditions. Data shown are from a representative out of two independent experiments. Data are expressed as mean ± SEM of three measurements, each collected in 2-8 replicates. **p < 0.01, ***p < 0.005, by Student t test, unpaired. **(F)** Magnetically purified Tregs and Tconvs were co-cultured at 1:1 ratio for 4 days with or without Etx (100 μM) or 2-DG (1 mM), stained with Bodipy and Foxp3, and analyzed by flow cytometry. Analysis of eFluor670 MFI or Bodipy gMFI (gated on proliferating cells) Tregs (red bars) or Tconvs (blue bars) is shown in the indicated conditions. Data shown as mean ± SEM; each condition was tested in triplicates; data shown are from a representative out of two independent experiments. *p < 0.05, **p < 0.01, ***p < 0.005, by Student t test, unpaired.

compared to TUM-Tconvs (**Fig. 3G**). Of note, *Pparg* and *Acacb* expression tended to co-segregate in all cell types and at higher levels in TUM-Tregs (**Fig. 3H**), suggesting a link between PPARγ expression and FAS program specifically in these cells.

Therefore, we tested whether TOFA, an inhibitor of acetyl-CoA carboxylase (ACC), key enzyme in FAS cascade, impacted on Treg proliferation. First, we administered TOFA to tumor-bearing mice, performing repeated intra-tumor injections starting when nodules were palpable: this treatment significantly suppressed tumor growth; however, this effect was unlikely due to immune-mediated events, as we failed to detect any significant increase in CD8 T cell frequency or IFNγ production in TOFA-treated compared to mock-treated nodules (SI Appendix, **Fig. S4A-B**). Rather, direct TOFA toxicity against tumor cells might account for the anti-tumor activity observed in vivo: indeed, TOFA reduced also in vitro the viability of the MCA38 cell line in a dose-dependent fashion, as evidenced in XTT cytotoxicity assay (SI Appendix, **Fig. S4C**).

To assess the role of FAS directly on Tregs, we took advantage of a model of Treg proliferation in vitro, which recapitulated

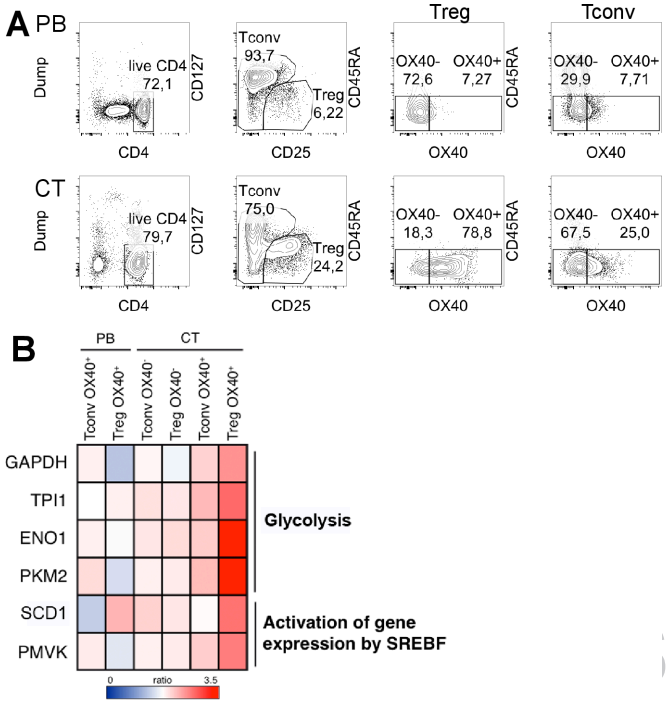

Fig. 7. *Human Treg proliferation, in vitro and ex vivo from diseased liver, is associated with glycolytic gene expression.* **(A-B)** OX40+/OX40- CD45RAlow Tregs and Tconvs were extracted and sorted from PB and cirrhosis/tumor (CT) of 5 patients with chronic HCV infection, and gene expression analysis was performed. **(A)** Sorting strategy. **(B)** The fold-change was calculated for each gene over the respective control (OX40- PB Tconvs for all Tconv samples, and OX40- PB Tregs for all Treg samples), and 216 genes upregulated >2fold only in Treg OX40+ CT were selected for pathway analysis (www.reactome.org). The heatmap displays the fold-change over control in the genes accounting for two pathways of interest, among those showing statistically significant enrichment ($p<0.05$).

the lipid accumulation occurring in TUM-Tregs in vivo. To this aim, Tregs were enriched from the spleens of naïve mice and polyclonally stimulated in vitro in the presence of IL-2: in this context, we could detect an increased incorporation in Tregs of the Bodipy lipophilic fluorophore, proportionally to IL-2 dosage and to the extent of proliferation **(Fig. 4A)**; notably, Bodipy levels were higher in proliferating than in resting cells, indicating active lipid accumulation during Treg cell division **(Fig. 4B)**. In this setting, TOFA treatment significantly inhibited, in a dose-dependent fashion, the proliferation of Tregs, and completely abolished FA accumulation selectively in proliferating cells, demonstrating a key role for FAS in both expansion and lipid pool generation of Tregs **(Fig. 4C)**. Of note, contrary to tumor cells, TOFA exposure did not exert a direct cytotoxic effect over Tconvs or Tregs, but rather increased their survival (SI Appendix, **Fig. S5)**.

To ascertain whether lipid accumulation and FAS reliance were preferential features of Tregs, we purified Tregs and Tconvs from spleens of naïve mice, labeled them with a proliferation tracer, and co-cultured them in the presence of IL-2: according to the literature (26), IL-2 supply allowed both Tregs and Tconvs to proliferate to a similar extent **(Fig. 4D)**. Here, in basal conditions, we found that Tregs showed significantly higher Bodipy content, yet same proliferation levels (as suggested by eFluor670 mean fluorescence intensity levels), compared to Tconvs, denoting that also in vitro Tregs were more prone to accumulate lipids during cell division; notably, the addition of TOFA significantly reduced proliferation and Bodipy staining in both Tregs and Tconvs, however Tregs were significantly more sensitive to such inhibition **(Fig. 4D-E)**.

Finally, we sought to test whether TOFA-treated Tregs were less able to suppress, when adoptively transferred in vivo, the immunity elicited by a primary growing tumors against a secondary challenge, i.e. "concomitant immunity" (27). To this aim, mice bearing palpable tumors received a second injection of tumor cells alone or admixed with TOFA- or mock-pretreated Tregs: the analysis of growing secondary tumors-infiltrating CD8 T cells revealed a trend for a decreased IFNγ and TNFα production in mice receiving tumor cells plus Tregs compared to tumor cells alone; notably, this suppressive effect was rescued when TOFA-treated Tregs were co-transferred with tumor cells (SI Appendix, **Fig. S6).** Together with in vitro data, these results point to a key role of FAS in Treg proliferation and possibly also in their suppressive function in vivo.

Glycolysis and fatty acids oxidation both concur to Treg advantage in cancer.

Memory CD8 T cells were shown to synthesize FAs from glucose (16), therefore we hypothesized that also Tregs might fuel FAS through a greater absorption of glucose, relative to effector T cells, which are instead damaged by glucose deprivation in the TME (17, 18). First, we analyzed, in Tregs and Tconvs from tumors and spleens, the expression of Glut1, a prominent glucose transporter in CD4 T cell activation (28) that is also relevant for Treg proliferation (12): we found that Glut1 was up-regulated in both Tconvs and Tregs at the TUM site, compared to SPL; however, such induction was significantly higher in Tregs, resulting in an increased relative ratio of Glut1 expression in Tregs versus Tconvs in tumors **(Fig. 5A-C)**. To directly track glucose uptake in vivo, we injected the fluorescent glucose analogue 2NBDG into tumor-bearing mice: in line with previous data (17, 18), Tconvs showed a massive defect in glucose uptake in TUM compared to SPL; conversely, Tregs displayed a relatively low glucose absorption in SPL that was maintained in TUM, resulting in a significant rescue of the Treg/Tconv relative ratio of glucose uptake at the tumor site **(Fig. 5D-F)**.

Then, we analyzed the expression of selected glycolysis-related genes (*Hk2*, *Gapdh*, and *Eno1*), through PrimeFlow RNA Assay, in Tregs and Tconvs: all 3 genes were significantly more represented in TUM-Tregs compared to TUM-Tconvs **(Fig. 5G)**. Interestingly, *Hk2* and *Eno1* (being the latter a master regulator of human Treg metabolism and development (11)), were repressed in tumors, compared to spleens, in both Tregs and Tconvs, in line with a general contraction of glycolysis in the tumor context; however, their expression remained higher in Tregs in both compartments, pointing to a preferential preservation of glycolytic activity in Tregs in the TME **(Fig. 5G, right)**.

The above results delineate a scenario in which Treg advantage in tumor may be sustained by the concomitant engagement of glucose and lipid metabolic routes. To address this aspect, we performed a metabolomic analysis of Tregs and Tconvs isolated from tumors or spleens: profoundly different profiles emerged from these T cell subsets **(Fig. 6A)**. In more detail, we could detect a series of metabolic changes in TUM-Tregs, compared to SPL-Tregs: TUM-Tregs displayed a preserved pentose phosphate (PP) pathway but higher glycolytic flux, higher consumption of acetyl-CoA and of the first intermediates of TCA cycle: citrate and α-ketoglutarate (SI Appendix, **Fig. S7A**). Of note, this profile was paralleled by increased NADH/NAD+ and NADPH/NADP+ ratios, and lower ATP/ADP ratios (SI Appendix, **Fig. S7B**), suggesting that in TUM-Tregs an improved glucose usage may fuel TCA cycle, whose intermediates are likely diverted to FA-biosynthetic pathways rather than being fully oxidized to generate ATP.

To functionally validate the peculiar TUM-Treg metabolic signature, we analyzed the bioenergetic profile of Tregs and Tconvs, isolated from SPL or TUM and cultured in vitro for 12 hours, through Seahorse assays. Basal glycolysis, as measured by extra-

cellular acidification rate (ECAR), in TUM compared to SPL, was repressed in Tconvs, as expected (18), but strikingly enhanced in Tregs (**Fig. 6B**). The rate of basal oxidative phosphorylation (OxPhos), as assessed by oxygen-consumption rate (OCR), was again inhibited in Tconvs at the tumor site, but maintained in Tregs (**Fig. 6C**). For all the metabolic indexes analyzed, Tregs showed a relative advantage over Tconvs specifically at the tumor site, as evidenced by higher Treg/Tconv ratios (**Fig. 6D-E**).

These data demonstrated that tumor-associated Tregs engage both glycolysis and OxPhos, for their expansion. To assess whether these metabolic routes are differentially required for Treg and Tconv proliferation, we performed the Treg/Tconv co-coculture assay described above, in the presence of 2DG or etomoxir (Etx), selective inhibitors of glycolysis or FAO, respectively. In line with previous results with human Tregs (14), 2DG profoundly restrained proliferation and lipid accumulation in both Tconvs and Tregs to a similar extent, suggesting that both cell types required glycolysis to support cell division and FAS; conversely, Etx affected, slightly though significantly, only Treg proliferation, and only in Tregs it promoted a further increase in Bodipy staining, indicating that FAO consumed the intracellular lipid pool and contributed to cell division specifically in Tregs (**Fig. 6F**). In analogy with the above-described effect of TOFA, we could not test also in vivo whether Etx blocked Treg proliferation in tumors, due to its direct toxicity against tumor cells that overshadowed any immune-mediated effect (**Fig. S3D-F**). However, the greater sensitivity to FAO blockade in vitro in the co-culture assay, and the higher rate of OxPhos ex vivo from tumors, together highlight the reliance of Tregs on FA utilization, and suggest that Tregs may display a relative resistance to glucose restriction in the TME due to their special ability to engage multiple metabolic routes, such as glycolysis and FA synthesis/oxidation.

Glycolytic and lipid biosynthetic pathways are active in human tumor-associated Tregs

Compared to mouse tumors, Tregs infiltrating human cancers display superior complexity and heterogeneity, which is not completely understood especially in immunometabolic aspects. Human cancer-infiltrating Tregs reveal a peculiar gene signature, characterized by specific chemokine receptors, immune checkpoints, and costimulatory molecules such as OX40 (29, 30). Based on our recent work, demonstrating that OX40-expressing Tregs were expanded in hepatic cirrhosis and liver and colon cancers, and that OX40 was connected to high proliferation, stability and suppression of tumor-associated Tregs (21, 22), we explored the gene signature of OX40+ Tregs, freshly extracted from specimens of liver cirrhosis and tumor (CT) or from peripheral blood (PB) of patients with chronic HCV infection and hepatocellular carcinoma (HCC), in comparison to OX40- Tregs and same subsets of Tconvs (**Fig. 7A**). We selected 216 genes showing a >2-fold increase selectively in CT OX40+ Tregs, and performed a pathway enrichment analysis: notably, among the significantly enriched pathways, we could reveal two metabolic routes, namely glycolysis ($p=0.00148$) and activation of gene expression by SREBF ($p=0.0466$) (**Fig. 7B** and SI Appendix, **Tables S1-S2**). Glycolysis-related genes included *GAPDH*, *TPI1*, *ENO1*, and *PKM2*, all involved in the glycolytic cascade, and *PKM2* in particular in substrate phosphorylation; the up-regulated genes belonging to the SREBF-related pathway were *SCD1* and *PMVK*, respectively involved in monounsaturated FA synthesis and in mevalonate pathway for cholesterol biosynthesis. In conclusion, these data demonstrate that also human Tregs shift between different metabolic routes in specific tissue contexts.

Discussion

The TME poses metabolic hurdles, such as hypoxia and glucose restriction, to the development of protective anti-tumor immunity. Nevertheless, this context favors the accumulation of proliferating and activated Tregs: our study demonstrates that such advantage may rely on their capacity to compete for glucose and perform FAS at higher rates compared to Tconvs.

Whether Tregs utilize glycolysis for their functions has been a matter of controversy in recent years. While it has been shown that murine iTregs (mostly polarized in the presence of TGFβ) show low glycolytic rates, and that glycolysis inhibition promotes their differentiation (7-10), human iTregs (differentiated with suboptimal stimulation) strictly rely on glycolysis for development and function (11). Human Tregs are highly glycolytic when freshly analyzed from human blood, and strongly require both FAO and glycolysis for their proliferation in vitro, while Tconvs rely only on glycolysis (13). Our present data confirm the same requirements in murine cells in vitro, and also demonstrate that Treg expansion in vivo in the tumor context is sustained by a strong increase in their glycolytic rate compared to Tconvs.

Others have shown that Glut1 is higher in proliferating Tregs from the spleens of naïve mice, and that Glut1 overexpression increased both glycolytic and oxidative metabolism in Tregs and provoked Treg expansion in the spleen; however, these Tregs showed signs of reduced stability and suppressive function (12, 28). These results suggest that an artificial boost in glycolysis may uncouple proliferation from suppressive function in Tregs. However, more and more data indicate that these two events are tightly interconnected, especially in tissue contexts where Tregs are activated: indeed, despite their refractoriness to conventional stimulation in vitro, Tregs are a highly proliferative population in vivo in both mice and humans, and many pieces of evidence demonstrate that activated Treg, displaying a higher proliferation rate, retain or even increase their suppressive ability in several contexts (31). Few examples are the spontaneous development of lethal autoimmunity due to impaired expansion of suppressive Tregs in mTORC1 deficiency (15), the impaired ability of OX40-null Tregs to suppress colitis because of defective competitive fitness (20), the ability of OX40/OX40L to induce the proliferation of highly suppressive human Tregs (21), and the lower proliferative potential of Tregs in multiple sclerosis patients with a more severe disease (32). In cancer mouse models and cancer patients, a huge amount of data demonstrates that highly proliferative and highly suppressive Tregs accumulate in tumors (2). Accordingly, our current results show, at the tumor site, higher frequency of Ki67+ and OX40+ Tregs, in association with increased glycolytic rate, higher Glut1 expression and improved competition for glucose. Combined with the well-established notion of the superior suppressive function of tumor-infiltrating Tregs, our data contribute to delineate a picture in which a glycolytic shift may boost proliferation and, consequently, suppressive function of Tregs in certain tissues and especially in cancer.

Foxp3 expression alone is sufficient to shift the metabolic program from glycolysis to oxidative phosphorylation, and enables Tregs to resist better to low-glucose, high-lactate exposure (12, 33): such default program may help Tregs to maintain their quiescent state in adverse conditions. However, our results indicate the presence of an active Treg proliferation in the tumor context, possibly sustained by glycolysis, and associated with the expression of OX40 as a marker of Treg activation; furthermore, OX40 engagement directly promotes the selective proliferation of lipid-laden Tregs in vivo. Overall, considering these results, it may be proposed that, on the one side, Foxp3 induces a default oxidative program to maintain Treg survival in a quiescent state; on the other side, the signal elicited through OX40, and possibly other costimulatory receptors and other members of the TNF receptor superfamily, may superimpose a glycolytic and anabolic boost over the oxidative program, allowing Tregs to exit from quiescence, undergo active proliferation and perform efficient suppressive function.

De novo synthesized intracellular lipids may be utilized not only for metabolic but also functional purposes. Lipids are a preferential source of acetyl groups for histone acetylation and epigenetic reprogramming (34), and short-chain FA uptake has been shown to support colonic Treg homeostasis through regulating histone acetylation (35, 36). The stability of Foxp3 itself is increased by acetylation (37) and may be thus sensitive to the supply of lipid-derived acetyl groups. Lipids are also necessary for the palmitoylation of crucial signaling proteins, for building cell membranes and shaping their lipid composition and fluidity, for the synthesis of pro- as well as anti-inflammatory lipid mediators. Our results suggest that TUM-Tregs may perform FAS not only to fuel FAO but also for other purposes. Indeed, the high neutral lipid content, and also the metabolite signature, observed in TUM-Tregs ex vivo indicates that FA synthesis may prevail over FA consumption; the glycolytic rate was boosted in TUM-Tregs to a greater extent when compared to oxidative indexes, and the co-induction of *Pparg* and *Acacb* was higher than *Cpt1a* increase in TUM-Tregs; finally, in vitro, Treg proliferation was more sensitive to the blockade of FAS than of FAO. Human OX40+ tumor-infiltrating Tregs displayed a gene signature oriented to glycolysis and lipid biosynthesis. Overall these data indicate that lipid biosynthetic pathways may dominate in active Treg expansion in cancer and also in inflammatory conditions; accordingly, impaired Treg homeostasis in mTORC1-deficient mice associates to defective lipid biosynthesis (15).

According to our gene expression analysis in OX40+ Tregs extracted from human tumor, a SREBP-driven program may support lipid biosynthesis in these cells. While no comprehensive data exist on the role of this family of transcription factors in Treg homeostasis and suppressive function, their function has been clearly elucidated in CD8 T cell activation: SREBP was essential for T cell transition from quiescence to activation through the active promotion of membrane synthesis (38). We would speculate that, likewise, a program of lipid biosynthesis, addressed to the construction of functional membranes, might support the local proliferation of OX40+ Tregs in the TME. Indeed, the two SREBP-related genes, *SCD1* and *PMVK*, upregulated in tumor OX40+ Tregs, may concur to the biosynthesis of those lipids, namely monounsaturated FAs and especially cholesterol, that more profoundly impact on membrane fluidity, lipid-raft formation and TCR clustering and signaling, as recently demonstrated in CD8 T cells (39).

We report here that OX40 triggering in naïve mice prompt the proliferation of lipid-laden Tregs: therefore, the OX40/OX40L signal, occurring in the HCC microenvironment (40), may directly sustain Treg lipogenic program. Indeed, OX40 ligation induces TRAF6 activation in CD4 T cells (41), and TRAF6 is a crucial driver of lipid metabolism in memory T cell development (42); therefore, we would suggest that the signal of OX40, possibly together with other TNF receptors, may sustain the transition of Tregs into the effector phase through the promotion of lipid biosynthetic pathways.

Our data show that Tregs accumulate intracellular lipids not only in cancer but also in a context of inflammation-driven expansion (early cholangitis in *Mdr2*$^{-/-}$ mice), but not in hepatic steatosis in the absence of inflammation (HCVTg mice at advanced age). Therefore, Treg lipid loading seems to occur as a result of Treg-intrinsic pathways (such as OX40 signaling) and irrespective of the lipid profile in the surrounding tissue. Intriguingly, we could find high expression of PPARγ also in TUM-Tregs. PPARγ is a nuclear factor that, in response to lipid ligands, controls a program of FA uptake, glucose uptake and lipogenesis in the adipose tissue, but also regulates a variety of other functions in other organs and in immune cells (43). In VAT-Tregs, PPARγ was shown to drive CD36 expression and FA incorporation; however, treatment of PPARγ-transfectants with a synthetic agonist induced not only *Cd36* gene, but also other genes involved in lipid metabolism, such as *Scd1* and *Cpt1a* among others (19). Therefore, PPARγ may be active in both VAT- and TUM-Tregs, driving a similar program of lipid rearrangement that is specifically instrumental to Treg expansion. Whether certain endogenous FAs, generated by lipogenesis, may bind (at relatively low affinity) and activate PPARγ, is still controversial (44). It is reasonable to think that PPARγ may be activated as a consequence of increased FAS in TUM-Tregs: in line with this hypothesis, we found a preferential co-segregation of *Pparg* and *Acacb* expression in TUM-Tregs.

At the systemic level, starvation leads to a transient Treg expansion through the mediation of the leptin/mTOR axis (13): indeed, conditions of poor nutrient availability may shift the balance from growth and defense to homeostasis maintenance, and switch the immune status from inflammation to immune regulation. We would propose that the tumor setting might configure as a context of nutrient starvation at the microenvironmental level, fostering immune regulatory events. Whether leptin deprivation plays a role in the local tumor-associated immune dysfunction, and especially in Treg expansion, remains to be investigated. While the link between obesity, chronic inflammation and cancer risk is well established, it is still unclear whether systemic/regional nutrient availability, adiposity or metabolic inflammation affects immune regulation at the tumor site; however, we have recently elucidated that OX40+ Tregs accumulate in the VAT of obese human subjects unless affected by colorectal cancer, suggesting that adipose tissue of obese individuals may represent a regional reservoir for Tregs to be recruited to the tumor site (45). Our present results suggest that perturbations in nutrient accessibility at the microenvironmental level may not only impact on tumor cell but also on immune cell functions. For instance, therapies targeting FAS, directly or indirectly, are under development for cancer treatment (46): based on our data, this approach may "off-target" Tregs, and especially activated tumor-associated Tregs, and it may thus act as a double-edge sword against both tumor cell proliferation and immune regulation.

Material and Methods

Tumor cell lines

MCA38 colon adenocarcinoma and B16F10 metastatic melanoma cell lines, kindly provided by M. P. Colombo (Fondazione IRCCS Istituto Nazionale Tumori, Milan, Italy), were cultured in complete Dulbecco's modified eagle medium (DMEM) with high glucose (Gibco) supplemented with 10% foetal bovine serum (FBS, Gibco), 2mM L-glutamine (Sigma-Aldrich), penicillin/streptomycin, non-essential aminoacids, sodium pyruvate (Euroclone), 50μM 2-mercaptoethanol (Sigma-Aldrich) and 10mM Hepes (Aurogene) at 37 °C in humidified 5% CO_2 atmosphere. To obtain transplanted tumors, tumor cells were subcutaneous injected into the right flank of C57BL/6NCrl wild-type male mice (Charles River Laboratories, Calco, Italy).

Mouse models

HCVTg mice (of the FL-N/35 transgenic lineage, expressing the HCV polyprotein under the albumin promoter (24)) were kindly provided by H. Lerat (Institut National de la Santé et de la Recherche Médicale, Unité U955, Université Paris-Est, Créteil) and backcrossed for more than 10 generations to the C57BL/6NCrl background before analysis. HCVTg and C57BL/6NCrl mice were bred and maintained under conventional conditions at animal facility of the Dipartimento di Scienze Anatomiche, Istologiche, Medico legali e dell'Apparato locomotore (SAIMLAL), in Sapienza Università di Roma, under protocols approved by the Italian Ministry of Health (Authorization #481/2015-PR). *Mdr2*$^{-/-}$ (FVB.129P2-*Abcb4* $^{tm1Bor/J}$) mice were obtained from the Jackson Laboratory and maintained under pathogen-free conditions at the Pasteur Institute animal facility (Paris). For all the experiments, mice were sacrificed by cervical dislocation. Tumor-bearing C57BL/6NCrl mice were sacrificed

after two weeks from subcutaneous tumor cell transplantation and tumor volume (mm^3) was calculated using the formula: (smaller diameter)^2 x larger diameter. For OX40 stimulation in vivo, C57BL/6 mice received intraperitoneal injection of 500 µg of anti-OX40 mAb (OX86, BioXcell); after 6 days, flow cytometry analysis was performed on splenocytes.

In vivo uptake assays

To test in vivo uptake of glucose and lipids, tumor-bearing mice received a single i.p. injection of 50 µg Bodipy-conjugated palmitate (Bodipy FL C16, Life Technologies), 1 hour before analysis, or a single i.p. injection of 100 µg fluorescent glucose analogue 2-NBDG (2-(N-(7-Nitrobenz-2-oxa-1,3-diazol-4-yl)Amino)-2-Deoxyglucose, Life Technologies), 15 minutes before analysis.

TOFA/Etx intra-tumor treatments

To test TOFA or Etx anti-tumor activity in vivo, tumor-bearing mice received repeated intra-tumor injections of 250 µg TOFA (Sigma) or 200 µg Etx (Sigma) at days 5, 8, 11 and 13 after s.c. tumor transplantation. As control, DMSO or water were administered, respectively; mice were sacrificed at day 14 for analysis.

All in vivo experiments were authorized by the institutional ethical committees and performed in accordance to institutional guidelines and national laws.

Lymphocyte extraction from murine tissues

Murine tumor samples were mechanically dissociated using gentleMACS Octo Dissociator according to manufacturer's instructions (Miltenyi Biotec), and mononuclear cells were enriched through 40/80 Percoll (GE Healthcare) density gradient, collecting cells at the interface between 40% and 80% Percoll solutions. The same protocol was applied for hepatic lymphocyte extraction. Splenocytes were obtained by spleen mechanical dissociation on 70-µm filter followed by ACK lysis buffer (Gibco) incubation for 4 minute at 4°C. Lymph nodes were mechanically dissociated on 70-µm filter. Cells were collected in complete RPMI-1640 Dutch modified medium containing 10% FBS (Gibco), 2 mM L-glutamine (Sigma-Aldrich), penicillin/streptomycin, non-essential aminoacids, sodium pyruvate (Euroclone), and 50 µM 2-mercaptoethanol (Sigma-Aldrich).

Flow cytometry and PrimeFlow RNA Assay

Bodipy (BODIPY™ 505/515, 4,4-Difluoro-1,3,5,7-Tetramethyl-4-Bora-3a,4a-Diaza-s-Indacene, ThermoFisher Scientific, catalog number D3921) is a cell membrane-permeant fluorophore specific for neutral lipid stores, known to stain lipid droplets in CD8 T cells (16). For Treg analysis, cells were incubated 15 minutes at 37°C with Fixable Viability Dye eFluor780 (eBioscience) plus Bodipy or Nile Red (Enzo Life Sciences) dyes for neutral lipid staining; then, staining with the following antibodies for surface antigens was performed for 20 minutes at 4°C: CD4 BrilliantViolet605, CD25 BrilliantViolet510 and CD134 (OX-40) BrilliantViolet421 (all from BioLegend), CD36 APC (BD Biosciences), Glut1 PE (Novus Biologicals). Finally, intracellular staining with Foxp3 PE-eFluor610 and Ki-67 PE-Cyanine7 (both from eBioscience) was performed for 30 minutes at RT, after cell fixation and permeabilization for 30 minutes at 4°C, using Foxp3/Transcription Factor Staining Buffer Set according to manufacturer's instructions (eBioscience). For CD8 analysis, cells were restimulated 4 hours with Cell Stimulation Cocktail plus Protein Transport Inhibitor (eBioscience), stained with Viability Dye eFluor780, CD8a BrilliantViolet785 (BioLegend), CD44 BrilliantViolet510 (BioLegend), fixed/permeabilized with Cytofix/Cytoperm solution according to manufacturer's instructions (BD Biosciences), and finally stained with IFNγ PE (eBioscience), TNFα PECy7 (Biolegend).

PrimeFlow RNA Assay (Affymetrix/eBioscience) was performed according to manufacturer's instructions. After surface staining and fixation/permeabilization, target probe hybridization was performed using type 1 (AlexaFluor647-conjugated) probes for *Pparg* and *Eno1* mRNAs, type 4 (AlexaFluor488-conjugated) probes for *Cpt1a* and *Hk2* mRNAs, and type 6 (AlexaFluor750-conjugated) probes for *Acacb* and *Gapdh* mRNAs. As a positive control, mouse beta Actin (*Actb*), conjugated with each probe type, was used. Cells were incubated for 2 hours with the target probes at 40°C in a thermal incubator for microtubes, then were incubated with the PreAmplification (PreAmp) reagent for 2 hours and the Amplification (Amp) reagent for an additional 2 hours at 40°C. After signal amplification, cells were incubated with label probes at 40°C for 1 hour and finally cells were washed and resuspended in staining buffer for acquisition.

Data were acquired on LSR Fortessa (Becton Dickinson) and analyzed with FlowJo software (Tree Star Inc, version 10.1r5).

In vitro proliferation assays

CD4+CD25+ Tregs and CD4+CD25- Tconvs were magnetically purified from splenocytes of wild-type C57BL/6 mice using the CD4+CD25+ Regulatory T Cell Isolation Kit (Miltenyi Biotec), labeled with 10 µM cell proliferation dye eFluor670 (eBioscience) by incubation for 15 minutes at 37°C in complete RPMI Dutch modified medium, and cultured or co-cultured at 1:1 ratios in presence of equal numbers of irradiated (3500 rad) autologous splenocytes plus soluble anti-CD3 (1 µg/ml, eBioscience) and IL-2 (100 IU/ml, Roche), and in presence or not of TOFA (Sigma), Etomoxir (Etx, Sigma) or 2-deoxy-D-glucose (2-DG, Sigma) at different concentrations. After 4 days of culture, analysis of eFluor670 dilution and Bodipy incorporation was performed in gated Foxp3+ (Tregs) or Foxp3- (Tconvs) by flow cytometry.

Adoptive Treg transfer and suppression of concomitant immunity in vivo

CD4+CD25+ Tregs were magnetically purified from splenocytes of wild-type C57BL/6 mice, and cultured for 40 hours in complete RPMI medium with coated anti-CD3 (1 µg/ml) plus IL-2 (100 IU/ml), in the presence of TOFA (5 µg/ml) or DMSO as control. Recipient mice first received a primary tumor inoculum of 10^5 MCA38 cells subcutaneously in the right flank. After 10 days, when primary tumors were palpable, mice received a challenge inoculum in the opposite flank, containing 10^5 MCA38 cells, either alone or admixed at 1:1 ratio with Tregs, prepared as described above. After further 13 days, flow cytometry was performed in lymphocytes extracted from draining lymph nodes and tumors.

Seahorse analysis

OCR and ECAR real-time measurements were performed using an XFe-96 Extracellular Flux Analyzer (Seahorse Bioscience) in basal condition in XF media and also in response to 5 µM oligomycin, 1.5 µM of carbonylcyanide-4- (trifluoromethoxy)-phenylhydrazone (FCCP), or 1 µM of Antimycin and Rotenone (all from Sigma-Aldrich) for OCR profile, whereas in response to 10 mM glucose, 5 µM oligomycin and 100 mM 2-DG (all from Sigma-Aldrich) for ECAR analysis. Basal OxPhos (before oligomycin addition) and ATP-linked OxPhos (as difference between basal OCR and oligomycin-induced OCR) were calculated from the OCR profile, as indices of mitochondrial respiratory function; basal glycolysis (after the addition of glucose), maximal glycolysis (after the addition of oligomycin), and glycolytic capacity (as difference between oligomycin-induced ECAR and 2-DG-induced ECAR) were calculated from the ECAR profile as indices of glycolytic pathway activation.

Metabolomic analysis

CD4+CD25+ Tregs and CD4+CD25- Tconvs were magnetically purified from pooled splenocytes and tumors of C57BL/6 mice (n=15) using the CD4+CD25+ Regulatory T Cell Isolation Kit (Miltenyi Biotec). Pellets were then resuspended in 250µl methanol/acetonitrile 1:1 containing [U-$^{13}C_6$]-Glucose- 1ng/µl

(internal standard, Sigma Aldrich, 389374) and lysed by Tissue lyser 3 min at the highest frequency. Lysates were spun at 20,000g for 5 min at 4°C. Supernatants were then passed through a regenerated cellulose filter, dried and resuspended in 100µl of MeOH for subsequent analysis. Metabolomic data were obtained on an API-4000 triple quadrupole mass spectrometer (AB Sciex) coupled with a HPLC system (Agilent) and CTC PAL HTS autosampler (PAL System). The identity of all metabolites was confirmed using pure standards. Quantification of different metabolites was performed with a liquid chromatography/tandem mass spectrometry (LC-MS/MS) method using cyano-phase LUNA column (50mm x 4.6mm, 5µm; Phenomenex). Methanolic samples were analyzed by a 5 min run in negative ion mode with 30 MRM transitions. The mobile phase A was: 5 mM ammonium acetate pH 7.00 in MeOH. The gradient was 100%A for all the analysis with a flow rate of 500µl/min. MultiQuant™ software (version 3.0.2) was used for data analysis and peak review of chromatograms. Quantitative evaluation of all metabolites was performed based on calibration curves with pure standards, then data were normalized on micrograms of proteins analyzed by Bradford method.

XTT cytotoxicity assay

To assess the cytotoxic effects of TOFA and Etx on tumor cells in vitro, MCA38 cells were seeded at the concentration of $5x10^3$ cells/well into 200 µl of complete DMEM medium in flat-bottomed 96-well plate, in presence of different concentrations of TOFA and Etx, or DMSO and water as respective controls. Conditions without cells or cell treatment with 0.05% saponin (Sigma-Aldrich) were used as negative and positive control, respectively. After 24 hours of culture, the analysis of cell viability was performed with XTT Cell Proliferation Assay Kit (Cayman Chemical), and absorbance was measured with Multiskan FC (Thermo Scientific).

Human samples

Peripheral blood from healthy volunteers was obtained from buffy coats of healthy blood donors, anonymously provided by the Immunohematology and Transfusion Center of Policlinico Umberto I. Peripheral blood and liver specimens were obtained from 5 patients with chronic hepatitis C, cirrhosis and hepatocellular carcinoma (4 males and 1 female, aged 53-80 years), undergoing surgery or liver transplantation at Istituto Nazionale dei Tumori "Regina Elena" or "Sapienza" Università di Roma - Policlinico Umberto I. Human studies have been performed in accordance to the ethical guidelines of the 1975 Declaration of Helsinki and were approved by the Institutional Ethical Committee (Authorization: RIF.CE: 4259). Informed consent was obtained from all patients.

Human Treg/Tconv sorting and gene expression analysis

Liver fragments from patients were perfused and grossly mashed with HBSS (Euroclone) containing 0.5 mg/ml collagenase IV (Sigma-Aldrich) and 50 ng/ml DNAse I (Worthington). Samples were incubated 10 minutes at 37°C and then mechanically disaggregated into single cell suspensions. Mononuclear cells were enriched by Lympholyte (Cederlane) density gradient, also from patient PB. T cells were enriched from mononuclear cells using Pan T cell Isolation kit II (Miltenyi Biotec) and, after treatment with Fixable Viability Dye eFluor780 (eBioscience) and with FcBlock (eBioscience) for 15 minutes at 4°C, were stained for surface markers: dump channel (CD14 APCeFluor780, CD56 APCeFluor780, CD8 APCeFluor780, all from eBioscience), CD4 AlexaFluor488 (eBioscience), OX40 PE (ACT35, BD), CD45RA PerCPCy5.5 (BioLegend), CD127 PECy7 (BioLegend) and CD25 APC (BioLegend). Therefore, OX40+ and OX40- subsets, in gated CD45RA low Tregs and Tconvs, were sorted using a FACSAria II (Becton Dickinson).

Total RNA was isolated using mirVana Isolation Kit (Ambion) following the standard protocol. Briefly, the lysates were extracted once with Acid-Phenol Chloroform and further purified to yield total RNA. Extracted RNA was quantified with RiboGreen Quantitation Kit (Molecular Probes) on an Infinite F200 plate reader (Tecan Trading AG). All extracted RNA samples were quality controlled for integrity with 2100 Bioanalyzer (Agilent Technologies).

Gene expression of whole transcriptomes was performed according to the standard protocol. Total RNA was isolated, quality controlled and quantified as described above; for each sample 100 ng of total RNA were reverse transcribed according to the Illumina TotalPrep RNA Amplification kit (Ambion) and biotinylated cRNA was generated by in vitro transcription. Washing, staining and hybridization were performed according to the standard Illumina protocol: briefly, 750 ng of cRNA of each sample in a final volume of 15 µl were hybridized onto Illumina HumanHT-12 v4 Expression BeadChip arrays. Hybridization and scanning were performed according to the manufacturer's indications on an Illumina iScan System and data were processed with BeadStudio v.3; arrays were quantile normalized, with no background subtraction, and average signals were calculated on gene-level data for genes whose detection p-value was lower than 0.001 in at least one sample.

Statistical analysis

Statistical analysis was performed using Prism software (version 6.0, GraphPad). Two tailed-unpaired Student's t test was used to analyze in vitro data and to compare ex vivo data from Tregs and Tconvs in different samples, while two tailed-paired Student's t test were applied to compare ex vivo data from Tregs and Tconvs in the same sample. Every in vitro and ex vivo assay was performed in duplicate, triplicate, or quadruplicate when possible and for all experiment the number of repetitions is indicated in the figure legend. In all graphs, bars show means ± SEM. In all tests, $P<0.05$ was considered statistically significant.

Acknowledgements: We would like to thank Massimo Rossi, Nicola Guglielmo, Gian Luca Grazi for liver specimens, Mario P. Colombo for providing mouse tumor cell lines, Natalia Pediconi and Massimo Levrero for discussion and for sharing reagents, Alfonso Grimaldi for collaboration in the revision process, Giovanni Bernardini for sharing reagents, and Hervé Lerat for providing HCVTg colony founders.

This work was supported by the following grants: AIRC IG-2014 15199 and AIRG IG-2017 19939 to VB; AIRC IG-2017 19784 to SP; MIUR RF-2010-2310438 and RF 2010-2318269; FISM onlus (cod. 2015/R/04 to VB; cod. 2013/R/9 to EMC and cod. 2014/R/19 to MS); MIUR PRIN 2010-2011 prot. 2010LC747T_004; FIRB-2011/13 no. RBAP10TPXK; Istituto Pasteur Italia – Fondazione Cenci Bolognetti (grant 2014-2016); International Network Institut Pasteur PTR n. 20-16; Fondazione Roma Grants for Biomedical Research NCDS-2013-000000345; the European Union's Seventh Framework Program (FP7) under grant agreement No. 259743 (MODHEP consortium) to YW; Fondazione Cariplo 2016-0852 (to GDN); Ministero della Salute GR-2011-02346974 (to GDN) and GR-2013-02355011 (to FB); grant from the European Union IDEAS Programme European Research Council Starting Grant "menTORingTregs" n. 310496 to GM. CF was supported by a 2015 Fellowship from Fondazione Veronesi. **Footnotes** [1]To whom correspondence may be addressed. Email: silvia.piconese@uniroma1.it, giuseppe.matarese@unina.it; vincenzo.barnaba@uniroma1.it. Author contributions: IP performed and analyzed most of the experiments, with the experimental support of CF and SM, and wrote the paper; ET collaborated in liver specimen processing; CP and DF performed Seahorse analysis; MS and FR, under the supervision of EMC, helped in experiments with human Tregs; FB, NM and GDN performed metabolomic analysis; GR conducted microarray experiments and VR performed bioinformatic analysis, under the supervision of MP; EG performed cell sorting; YW provided samples and support with *Mdr2*$^{-/-}$ mice; VB supervised project development and contributed to write the paper; GM provided substantial contribution to project design and paper writing; SP conceptualized the study, performed and analyzed the experiments and wrote the paper. Competing interests: The authors declare no no conflict of interest. Data deposition: The microarray dataset has been deposited in GEO under the Accession Number GSE103523.

1. Roychoudhuri R, Eil RL, & Restifo NP (2015) The interplay of effector and regulatory T

cells in cancer. *Curr Opin Immunol* 33:101-111.
2. Burocchi A, Colombo MP, & Piconese S (2013) Convergences and divergences of thymus- and peripherally derived regulatory T cells in cancer. *Front Immunol* 4:247.
3. Kretschmer K, Apostolou I, Hawiger D, Khazaie K, Nussenzweig MC, & von Boehmer H (2005) Inducing and expanding regulatory T cell populations by foreign antigen. *Nat Immunol* 6(12):1219-1227.
4. Weiss JM, Bilate AM, Gobert M, Ding Y, Curotto de Lafaille MA, Parkhurst CN, Xiong H, Dolpady J, Frey AB, Ruocco MG, Yang Y, Floess S, Huehn J, Oh S, Li MO, Niec RE, Rudensky AY, Dustin ML, Littman DR, & Lafaille JJ (2012) Neuropilin 1 is expressed on thymus-derived natural regulatory T cells, but not mucosa-generated induced Foxp3+ T reg cells. *J Exp Med* 209(10):1723-1742, S1721.
5. Zhou G & Levitsky HI (2007) Natural regulatory T cells and de novo-induced regulatory T cells contribute independently to tumor-specific tolerance. *J Immunol* 178(4):2155-2162.
6. Pearce EL, Poffenberger MC, Chang CH, & Jones RG (2013) Fueling immunity: insights into metabolism and lymphocyte function. *Science* 342(6155):1242454.
7. Berod L, Friedrich C, Nandan A, Freitag J, Hagemann S, Harmrolfs K, Sandouk A, Hesse C, Castro CN, Bahre H, Tschirner SK, Gorinski N, Gohmert M, Mayer CT, Huehn J, Ponimaskin E, Abraham WR, Muller R, Lochner M, & Sparwasser T (2014) De novo fatty acid synthesis controls the fate between regulatory T and T helper 17 cells. *Nat Med* 20(11):1327-1333.
8. Michalek RD, Gerriets VA, Jacobs SR, Macintyre AN, MacIver NJ, Mason EF, Sullivan SA, Nichols AG, & Rathmell JC (2011) Cutting edge: distinct glycolytic and lipid oxidative metabolic programs are essential for effector and regulatory CD4+ T cell subsets. *J Immunol* 186(6):3299-3303.
9. Shi LZ, Wang R, Huang G, Vogel P, Neale G, Green DR, & Chi H (2011) HIF1alpha-dependent glycolytic pathway orchestrates a metabolic checkpoint for the differentiation of TH17 and Treg cells. *J Exp Med* 208(7):1367-1376.
10. Gerriets VA, Kishton RJ, Nichols AG, Macintyre AN, Inoue M, Ilkayeva O, Winter PS, Liu X, Priyadharshini B, Slawinska ME, Haeberli L, Huck C, Turka LA, Wood KC, Hale LP, Smith PA, Schneider MA, MacIver NJ, Locasale JW, Newgard CB, Shinohara ML, & Rathmell JC (2015) Metabolic programming and PDHK1 control CD4+ T cell subsets and inflammation. *J Clin Invest* 125(1):194-207.
11. De Rosa V, Galgani M, Porcellini A, Colamatteo A, Santopaolo M, Zuchegna C, Romano A, De Simone S, Procaccini C, La Rocca C, Carrieri PB, Maniscalco GT, Salvetti M, Buscarinu MC, Franzese A, Mozzillo E, La Cava A, & Matarese G (2015) Glycolysis controls the induction of human regulatory T cells by modulating the expression of FOXP3 exon 2 splicing variants. *Nat Immunol* 16(11):1174-1184.
12. Gerriets VA, Kishton RJ, Johnson MO, Cohen S, Siska PJ, Nichols AG, Warmoes MO, de Cubas AA, MacIver NJ, Locasale JW, Turka LA, Wells AD, & Rathmell JC (2016) Foxp3 and Toll-like receptor signaling balance Treg cell anabolic metabolism for suppression. *Nat Immunol* 17(12):1459-1466.
13. Procaccini C, De Rosa V, Galgani M, Abanni L, Cali G, Porcellini A, Carbone F, Fontana S, Horvath TL, La Cava A, & Matarese G (2010) An oscillatory switch in mTOR kinase activity sets regulatory T cell responsiveness. *Immunity* 33(6):929-941.
14. Procaccini C, Carbone F, Di Silvestre D, Brambilla F, De Rosa V, Galgani M, Faicchia D, Marone G, Tramontano D, Corona M, Alviggi C, Porcellini A, La Cava A, Mauri P, & Matarese G (2016) The Proteomic Landscape of Human Ex Vivo Regulatory and Conventional T Cells Reveals Specific Metabolic Requirements. *Immunity* 44(2):406-421.
15. Zeng H, Yang K, Cloer C, Neale G, Vogel P, & Chi H (2013) mTORC1 couples immune signals and metabolic programming to establish T(reg)-cell function. *Nature* 499(7459):485-490.
16. O'Sullivan D, van der Windt GJ, Huang SC, Curtis JD, Chang CH, Buck MD, Qiu J, Smith AM, Lam WY, DiPlato LM, Hsu FF, Birnbaum MJ, Pearce EJ, & Pearce EL (2014) Memory CD8(+) T cells use cell-intrinsic lipolysis to support the metabolic programming necessary for development. *Immunity* 41(1):75-88.
17. Ho PC, Bihuniak JD, Macintyre AN, Staron M, Liu X, Amezquita R, Tsui YC, Cui G, Micevic G, Perales JC, Kleinstein SH, Abel ED, Insogna KL, Feske S, Locasale JW, Bosenberg MW, Rathmell JC, & Kaech SM (2015) Phosphoenolpyruvate Is a Metabolic Checkpoint of Anti-tumor T Cell Responses. *Cell* 162(6):1217-1228.
18. Chang CH, Qiu J, O'Sullivan D, Buck MD, Noguchi T, Curtis JD, Chen Q, Gindin M, Gubin MM, van der Windt GJ, Tonc E, Schreiber RD, Pearce EJ, & Pearce EL (2015) Metabolic Competition in the Tumor Microenvironment Is a Driver of Cancer Progression. *Cell* 162(6):1229-1241.
19. Cipolletta D, Feuerer M, Li A, Kamei N, Lee J, Shoelson SE, Benoist C, & Mathis D (2012) PPAR-gamma is a major driver of the accumulation and phenotype of adipose tissue Treg cells. *Nature* 486(7404):549-553.
20. Piconese S, Pittoni P, Burocchi A, Gorzanelli A, Care A, Tripodo C, & Colombo MP (2010) A non-redundant role for OX40 in the competitive fitness of Treg in response to IL-2. *Eur J Immunol* 40(10):2902-2913.
21. Piconese S, Timperi E, Pacella I, Schinzari V, Tripodo C, Rossi M, Guglielmo N, Mennini G, Grazi GL, Di Filippo S, Brozzetti S, Fazzi K, Antonelli G, Lozzi MA, Sanchez M, & Barnaba V (2014) Human OX40 tunes the function of regulatory T cells in tumor and nontumor areas of hepatitis C virus-infected liver tissue. *Hepatology* 60(5):1494-1507.
22. Timperi E, Pacella I, Schinzari V, Focaccetti C, Sacco L, Farelli F, Caronna R, Del Bene G, Longo F, Ciardi A, Morelli S, Vestri AR, Chirletti P, Barnaba V, & Piconese S (2016) Regulatory T cells with multiple suppressive and potentially pro-tumor activities accumulate in human colorectal cancer. *Oncoimmunology* 5(7):e1175800.
23. Mauad TH, van Nieuwkerk CM, Dingemans KP, Smit JJ, Schinkel AH, Notenboom RG, van den Bergh Weerman MA, Verkruisen RP, Groen AK, Oude Elferink RP, & et al. (1994) Mice with homozygous disruption of the mdr2 P-glycoprotein gene. A novel animal model for studies of nonsuppurative inflammatory cholangitis and hepatocarcinogenesis. *Am J Pathol* 145(5):1237-1245.
24. Lerat H, Honda M, Beard MR, Loesch K, Sun J, Yang Y, Okuda M, Gosert R, Xiao SY, Weinman SA, & Lemon SM (2002) Steatosis and liver cancer in transgenic mice expressing the structural and nonstructural proteins of hepatitis C virus. *Gastroenterology* 122(2):352-365.
25. Ruby CE, Yates MA, Hirschhorn-Cymerman D, Chlebeck P, Wolchok JD, Houghton AN, Offner H, & Weinberg AD (2009) Cutting Edge: OX40 agonists can drive regulatory T cell expansion if the cytokine milieu is right. *J Immunol* 183(8):4853-4857.
26. Thornton AM, Donovan EE, Piccirillo CA, & Shevach EM (2004) Cutting edge: IL-2 is critically required for the in vitro activation of CD4+CD25+ T cell suppressor function. *J Immunol* 172(11):6519-6523.
27. Turk MJ, Guevara-Patino JA, Rizzuto GA, Engelhorn ME, Sakaguchi S, & Houghton AN (2004) Concomitant tumor immunity to a poorly immunogenic melanoma is prevented by regulatory T cells. *J Exp Med* 200(6):771-782.
28. Macintyre AN, Gerriets VA, Nichols AG, Michalek RD, Rudolph MC, Deoliveira D, Anderson SM, Abel ED, Chen BJ, Hale LP, & Rathmell JC (2014) The glucose transporter Glut1 is selectively essential for CD4 T cell activation and effector function. *Cell Metab* 20(1):61-72.
29. De Simone M, Arrigoni A, Rossetti G, Gruarin P, Ranzani V, Politano C, Bonnal RJ, Provasi E, Sarnicola ML, Panzeri I, Moro M, Crosti M, Mazzara S, Vaira V, Bosari S, Palleschi A, Santambrogio L, Bovo G, Zucchini N, Totis M, Gianotti L, Cesana G, Perego RA, Maroni N, Pisani Ceretti A, Opocher E, De Francesco R, Geginat J, Stunnenberg HG, Abrignani S, & Pagani M (2016) Transcriptional Landscape of Human Tissue Lymphocytes Unveils Uniqueness of Tumor-Infiltrating T Regulatory Cells. *Immunity* 45(5):1135-1147.
30. Plitas G, Konopacki C, Wu K, Bos PD, Morrow M, Putintseva EV, Chudakov DM, & Rudensky AY (2016) Regulatory T Cells Exhibit Distinct Features in Human Breast Cancer. *Immunity* 45(5):1122-1134.
31. Attridge K & Walker LS (2014) Homeostasis and function of regulatory T cells (Tregs) in vivo: lessons from TCR-transgenic Tregs. *Immunol Rev* 259(1):23-39.
32. Carbone F, De Rosa V, Carrieri PB, Montella S, Bruzzese D, Porcellini A, Procaccini C, La Cava A, & Matarese G (2014) Regulatory T cell proliferative potential is impaired in human autoimmune disease. *Nat Med* 20(1):69-74.
33. Angelin A, Gil-de-Gomez L, Dahiya S, Jiao J, Guo L, Levine MH, Wang Z, Quinn WJ, 3rd, Kopinski PK, Wang L, Akimova T, Liu Y, Bhatti TR, Han R, Laskin BL, Baur JA, Blair IA, Wallace DC, Hancock WW, & Beier UH (2017) Foxp3 Reprograms T Cell Metabolism to Function in Low-Glucose, High-Lactate Environments. *Cell Metab* 25(6):1282-1293 e1287.
34. McDonnell E, Crown SB, Fox DB, Kitir B, Ilkayeva OR, Olsen CA, Grimsrud PA, & Hirschey MD (2016) Lipids Reprogram Metabolism to Become a Major Carbon Source for Histone Acetylation. *Cell Rep* 17(6):1463-1472.
35. Arpaia N, Campbell C, Fan X, Dikiy S, van der Veeken J, deRoos P, Liu H, Cross JR, Pfeffer K, Coffer PJ, & Rudensky AY (2013) Metabolites produced by commensal bacteria promote peripheral regulatory T-cell generation. *Nature* 504(7480):451-455.
36. Furusawa Y, Obata Y, Fukuda S, Endo TA, Nakato G, Takahashi D, Nakanishi Y, Uetake C, Kato K, Kato T, Takahashi M, Fukuda NN, Murakami S, Miyauchi E, Hino S, Atarashi K, Onawa S, Fujimura Y, Lockett T, Clarke JM, Topping DL, Tomita M, Hori S, Ohara O, Morita T, Koseki H, Kikuchi J, Honda K, Hase K, & Ohno H (2013) Commensal microbe-derived butyrate induces the differentiation of colonic regulatory T cells. *Nature* 504(7480):446-450.
37. van Loosdregt J & Coffer PJ (2014) Post-translational modification networks regulating FOXP3 function. *Trends Immunol* 35(8):368-378.
38. Kidani Y, Elsaesser H, Hock MB, Vergnes L, Williams KJ, Argus JP, Marbois BN, Komisopoulou E, Wilson EB, Osborne TF, Graeber TG, Reue K, Brooks DG, & Bensinger SJ (2013) Sterol regulatory element-binding proteins are essential for the metabolic programming of effector T cells and adaptive immunity. *Nat Immunol* 14(5):489-499.
39. Yang W, Bai Y, Xiong Y, Zhang J, Chen S, Zheng X, Meng X, Li L, Wang J, Xu C, Yan C, Wang L, Chang CC, Chang TY, Zhang T, Zhou P, Song BL, Liu W, Sun SC, Liu X, Li BL, & Xu C (2016) Potentiating the antitumour response of CD8(+) T cells by modulating cholesterol metabolism. *Nature* 531(7596):651-655.
40. Piconese S, Valzasina B, & Colombo MP (2008) OX40 triggering blocks suppression by regulatory T cells and facilitates tumor rejection. *J Exp Med* 205(4):825-839.
41. Xiao X, Balasubramanian S, Liu W, Chu X, Wang H, Taparowsky EJ, Fu YX, Choi Y, Walsh MC, & Li XC (2012) OX40 signaling favors the induction of T(H)9 cells and airway inflammation. *Nat Immunol* 13(10):981-990.
42. Pearce EL, Walsh MC, Cejas PJ, Harms GM, Shen H, Wang LS, Jones RG, & Choi Y (2009) Enhancing CD8 T-cell memory by modulating fatty acid metabolism. *Nature* 460(7251):103-107.
43. Ahmadian M, Suh JM, Hah N, Liddle C, Atkins AR, Downes M, & Evans RM (2013) PPARgamma signaling and metabolism: the good, the bad and the future. *Nat Med* 19(5):557-566.
44. Bensinger SJ & Tontonoz P (2008) Integration of metabolism and inflammation by lipid-activated nuclear receptors. *Nature* 454(7203):470-477.
45. Donninelli G, Del Cornò M, Pierdominici M, Scazzocchio B, Varì R, Varano B, Pacella I, Piconese S, Barnaba V, D'Archivio M, Masella R, Conti L, & Gessani S (2017) Distinct Blood and Visceral Adipose Tissue Regulatory T Cell and Innate Lymphocyte Profiles Characterize Obesity and Colorectal Cancer. *Front Immunol* 8:643.
46. Rohrig F & Schulze A (2016) The multifaceted roles of fatty acid synthesis in cancer. *Nat Rev Cancer* 16(11):732-749.